J Biomol NMR (2008) 42:129–137
DOI 10.1007/s10858-008-9270-2

ARTICLE

# Alternate HMQC experiments for recording HN and HC-correlation spectra in proteins at high throughput

**Luciano Mueller**

Received: 22 April 2008 / Accepted: 13 August 2008 / Published online: 27 September 2008


**Abstract** Alternate implementations of the SOFAST-HMQC experiment are described. In these alternate SOFAST-HMQC experiments (ALSOFAST-HMQC) excitation of the magnetization of interest is achieved by non-selective rf pulses while preserving the equilibrium polarization of passive spins. This alternate excitation scheme also allows the incorporation of a novel sensitivity enhancement protocol which has been most recently developed by Brutscher and coworkers and which permits simultaneous detection of both the x- and y-components of the indirectly detected $t_1$-interferograms without the need to introduce additional rf pulses and delays. We show that the ALSOFAST HC-HMQC experiment, which implements an alternate means of frequency selection, enables the detection of methyl resonances with large secondary proton chemical shifts. This is achieved by selecting coherences of interest via a frequency selective carbon inversion pulse. Detailed comparisons between SOFAST- and the presented ALSOFAST-HMQC experiment reveals a considerable degree of mutual complementarity.

**Keywords** NMR · HMQC · SOFAST · ALSOFAST · Indirect detection · Rapid data acquisition · Amino acid type editing · Paramagnetic relaxation agent · Sensitivity enhanced detection

**Electronic supplementary material** The online version of this article (doi:10.1007/s10858-008-9270-2) contains supplementary material, which is available to authorized users.

L. Mueller (✉)
Bristol-Myers Squibb, P.O. Box 4000, Route 206 and Province Line Road, 08543-4000 Princeton, NJ, USA
e-mail: luciano.mueller@bms.com

## Introduction

Multidimensional heteronuclear NMR experiments have revolutionized the utility of NMR spectroscopy as a research tool in biology and chemistry. The power of multidimensional NMR stems from the great flexibility by which magnetization can be shuffled among magnetically active nuclei within a molecule and the ability to indirectly detect spectral resonances. Indirect detection, however, comes with a penalty, that being the time required to complete the acquisition of a single data set is dramatically lengthened due to the need to repeat the acquisition of data a large number of times to map indirectly detected spectral interferograms.

In recent years many research efforts have focused on minimizing the time needed to acquire multidimensional heteronuclear NMR datasets. This has resulted in a plethora of novel data acquisition schemes. Thorough reviews of these high through-put NMR approaches are provided by (Freeman and Kupce 2003; Atreya and Szyperski 2005). Most recently, Schanda et al. introduced the SOFAST approach which minimizes saturation of nuclear magnetization during a multidimensional NMR experiment (Schanda and Brutscher 2005; Schanda et al. 2005; Kern et al. 2008). The SOFAST HN- or HC-HMQC experiments harness the sensitivity gains from optimized excitation of the nuclei of interest while minimizing the saturation of all passive protons. SOFAST-HMQC employs relaxation- or Ernst angle-optimized (Ernst and Anderson 1966) excitation of heteronuclear coherence (Ross et al. 1997), and by preserving magnetization of passive protons by longitudinal magnetization optimization (Pervushin et al. 2002). In particular, the preserved z-magnetization of passive protons provides an additional source of magnetization during a SOFAST experiment. In this report modifications to the

SOFAST-HMQC experiment are introduced. The key difference between SOFAST-HMQC and the presented ALSOFAST-HMQC experiment is in the way one excites hetero multiple quantum coherences. In SOFAST a frequency selective pulse is used to achieve Ernst angle (Ernst and Anderson 1966) optimized excitation of heteronuclear quantum coherence. In the current report, it is shown that the original INEPT-type excitation scheme of heteronuclear multiple quantum coherence achieves an equivalent MQ-excitation profile using only "hard' non-selective radio frequency pulses (Mueller 1979). This approach of scaling the excitation of magnetization of interest has been most recently reported by Kupce et al. (Kupce and Freeman 2007).

## ALSOFAST-HMQC experiments

### General features of the ALSOFAST-HMQC and comparisons with the SOFAST-HMQC

The pulse sequence of the ALSOFAST HN- or HC-HMQC experiment is depicted in Fig. 1. Instead of a frequency selective PC9-pulse, the heteronuclear multiple quantum coherence of interest is excited with a classical INEPT pulse cascade (Mueller 1979; Freeman et al. 1981). The proton coherence at point (e) in the pulse sequence (Fig. 1) is proportional to

$$\begin{aligned} &H_x(\text{NH or CH}) * (N_y \text{ or } C_y) * M_o * \sin(\pi * \tau_{hx} * J_{hx}) \\ &\quad + H_z(\text{NH and/or CH}) * M_o * \cos(\pi * \tau_{hx} * J_{hx}) \\ &\quad + H_z(\text{other}) \end{aligned} \quad (1)$$

This excitation scheme allows the selection of an arbitrary excitation flip angle for the magnetization of interest by choosing a desired INEPT mixing interval $\tau_{hx}$. For example, by setting $\tau_{hx}$ to 2/3 of $1/(2 * J_{hx})$ an excitation flip angle of 60° is achieved which corresponds to an 120° flip angle of the PC9 excitation pulse in the SOFAST experiment. This excitation scheme is related to the excitation pulse cascade in the longitudinal TROSY (Pervushin et al. 2002), where the magnetization of carbon-coupled protons are converted into $H_zC_z$ longitudinal magnetization at the start of the $t_1$-evolution period. In contrast to the longitudinal TROSY experiment, the ALSOFAST excitation scheme converts all non-NH magnetization into Hz-magnetization at point (e) (Fig. 1) regardless of whether the protein sample is [$^{15}$N] or [$^{13}$C,$^{15}$N]-labeled.

The first term in Eq. 1 then evolves in $t_1$ under proton decoupling, followed by a reverse INEPT transfer step (between points g and l in Fig. 1a, b). In order to ensure efficient water flip-back, an excitation sculpting pulse scheme (Hwang and Shaka 1995) is integrated into the experiment by the insertion of soft proton 180°-pulses at the end of each hard proton echo pulse (points f and j in Fig. 1a, b). To impart enhanced flexibility and slightly higher sensitivity and a moderately reduced suppression of the water peak, the gradient pulses flanking the proton 180°-pulse at point f in Fig. 1 (Hwang and Shaka 1995) has been eliminated in the pulse sequence which is depicted in Fig. 1. A variant pulse sequence which includes the first gradient pulse pair is depicted in the supplemental material. At the start of the acquisition period the magnetization of all passive spins, including the protons of the bulk water, are aligned along the z-axis, thereby minimizing the saturation of magnetization during a single scan. This alternate implementation of the SOFAST experiment offers two distinct advantages. First, the use of non-selective rf pulses affords a uniform excitation of all magnetization of interest. Second, by permitting frequency independent excitation, the ALSOFAST pulse sequence offers the flexibility of exciting targeted nitrogen or carbon excitation bands.

The enhanced excitation profiles of the ALSOFAST HN- and HC-HMQC experiments are illustrated in Figs. 2 and 3. Figure 2, which depicts expanded regions of spectra acquired with the SOFAST (Fig 2a) and ALSOFAST- (Fig. 2b) HN-HMQC excitation schemes, highlights the enhanced excitation of the resonance at 5.8 ppm. Figure 3 illustrates the enhanced excitation band width obtained with the ALSOFAST HC-HMQC excitation scheme where the selection of $^{13}$C-coherence of interest is achieved by a frequency selective G3-pulse (Emsley et al. 1990) (applied at point c in Fig. 1). The utilization of a frequency selective G3 $^{13}$C population inversion pulse in the ALSOFAST excitation scheme enables the methionine resonances around 2 ppm to be efficiently excited whereas these resonances are outside the range of excitation of the PC9-RSNOB pulse cascade in the SOFAST HC-HMQC experiment (Fig 3a).

In close analogy to the Sensitivity enhanced SOFAST-HMQC, the ALSOFAST-HMQC excitation scheme also permits the simultaneous detection of both the x- and y-component of the $t_1$-interferogram without the any additions of rf pulses or delays. Details of the sensitivity enhanced ALSOFAST-HMQC are depicted in detail below.

In comparison to the SOFAST-HMQC, the ALSOFAST-HMQC technique suffers from a couple of drawbacks which adversely impact its sensitivity. The key strength of the SOFAST-HMQC method lays in its simplicity, since it contains only two proton rf pulses producing a total rotation of proton magnetization of 300°. In contrast, ALSOFAST features two 90° pulses and three 180° pulses on the proton channel, resulting in a total rotation angle of 720°. In addition, the non-selective proton rf pulses in the ALSOFAST experiment temporarily flip the magnetization of all protons out of their equilibrium

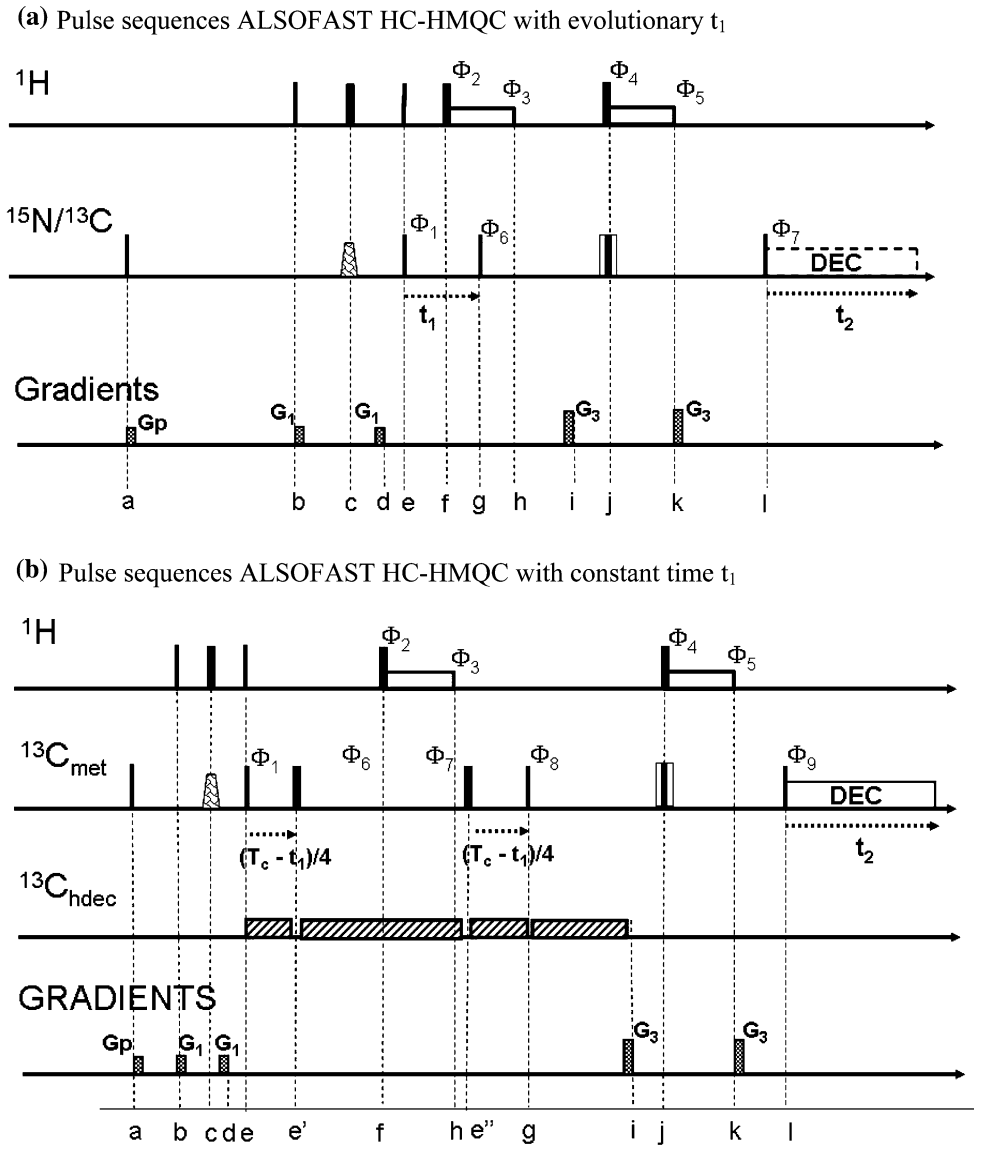


**Fig. 1** Pulse sequences of ALSOFAST HX-HMQC. (**a**) ALSOFAST HX-HMQC with evolutionary $t_1$. Time intervals: b–a = relaxation delay, c–b = e–c =($\alpha$/90) * 1/4 * $J_{xh}$), e–d = j–i = gradient pulse recovery delay, f–e = g–f = $t_1$/2, j–g = l–j = 1/(4 * $J_{xh}$), k–j = pwwg. Phase tables: Φ1 = x, −x; receiver = x, −x, −x, x; Φ2 = x, x, y, y; Φ3 = −x, −x, −y, −y; Φ4 = x; Φ5 = −x, Φ6 = x and −y for detecting x- and y-component of the $t_1$-interferogram, respectively, Φ7 = 4x, 4−x ($^{15}$N-decoupling mode). Sensitivity enhanced mode: Φ6 = x, x, −y, −y, and Φ7 = y, −y, x, −x, for fid 1–4 per $t_1$-point, respectively, no X-decoupling, the hashed trapezoidal shaped pulse in $^{13}$C/$^{15}$N-channel at point c represents a composite $90_x240_y90_x$-pulse in $^{15}$N-correlation and a G3-pulse with 20 ppm inversion width in the $^{13}$C-methyl correlation experiment, the concentric pair of open and solid rectangles at point j on the line $^{15}$N/$^{13}$C in Fig. 1a and $^{13}$Cmet in Fig. 1b represent a composite $90_x240_y90_x$-pulse. Gradient pulses: Gp = 12 G/cm, G1 = 2 G/cm, G3 = 24 G/cm, $gt_1$ = 0.5 ms, $gt_3$ = 0.2 ms, optional $^{13}$C decoupling in $^{15}$N-correlation with composite $^{13}$C-decoupling pulse at 110 ppm at time point f. The dashed square to the right of point j indicate the application of inverse decoupling in the non-sensitivity enhanced implementation of the experiment. X-nucleus carrier frequency: $^{15}$N-correlation = 118 ppm, $^{13}$C-methyl correlation 16 ppm. $^{13}$C-decoupling: wurst40 with a 25 ppm band width and an inversion pulse duration of 2.0 ms, $^{15}$N-decoupling: wurst40 with a 40 ppm band width and a 2.1 ms inversion pulse width. (**b**) ALSOFAST HC-HMQC with constant $t_1$-evolution. Time intervals: b–a = relaxation delay, c–b = e–c = ($\alpha$/90) * (1/4 * $J_{ch}$), e–d = gradient pulse recovery delay, e'–e = g–e" = $T_c$/4 − $t_1$/4 + pwC, g–e = $T_c$ = 1/(2 * $J_{HC}$), j–g = 1/(4 * $J_{ch}$), k–j = pwwg, pwwg is the duration of the Excitation Sculpting soft inversion pulse, phase tables: $\Phi_1$ = x, receiver = x, −x, −x, x, −x, x, x, −x, $\Phi_2$ = x, x, y, y, $\Phi_3$ = −x, −x, −y, −y, $\Phi_4$ = x, $\Phi_5$ = −x, $\Phi_6$ = x, y, $\Phi_7$ = 4x, 4y, $\Phi_8$ = x (−y) for x- and y- component of $t_1$-interferogram, $\Phi_9$ = 8x, 8(−x). Gradient pulses: Gp = 12 G/cm, G1 = 2 G/cm, G3 = 24 G/cm, $gt_1$ = 0.5 ms, $gt_3$ = 0.2 ms. Proton frequency = water resonance frequency, $^{13}$C frequency = 16 ppm. Residue-selection by $^{13}$C-homodecoupling in constant time evolution period: Methionine: No homo-decoupling Threonine: CA-wurst bw = 10 p at 71.0 and −39 ppm, inversion pulse width = 5 ms. Alanine: CA-wurst bw = 12 p at 53.0 and −21.0 ppm, inversion pulse width = 5 ms. Valine: CA-wurst bw = 12 p at 36.0 and −4.0 ppm, inversion pulse width = 5 ms. 4 ppm band selective: CA-WURST, bw = 4 ppm at selected carbon frequency + mirror image frequency (the mirror image adiabatic sweeps employ opposite frequency sweeps)

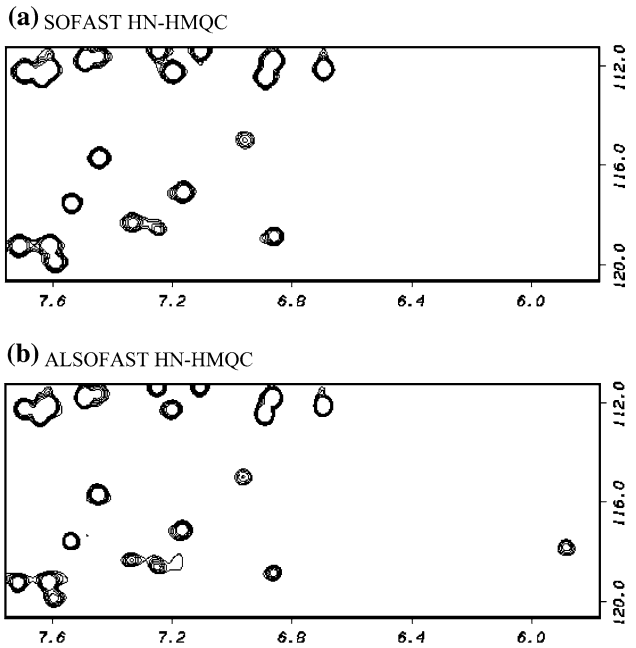


**Fig. 2** High field region of (**a**) SOFAST HN-HMQC and (**b**) ALSOFAST HN-HMQC in 0.36 mM [$^{13}$C,$^{15}$N]-FKBP-12, $sw_1 = 2{,}100$, $sw = 11{,}000$, $t_1max = 42$ ms, $t_2$-acquisition time = 60 ms, data collection time of 2.1 min, relaxation delay of 0.23 s, temp 20°C, recorded on Inova 600 MHz spectrometer with cold probe. In SOFAST the excitation pulse was a PC9-pulse resonating at 8.2 ppm with a 4 ppm band width and an excitation angle of 120° and the refocusing pulse was a REBURP-pulse resonating at 8.2 ppm with an inversion band width of 4 ppm. In ALSOFAST the excitation flip angle $\alpha = 60°$

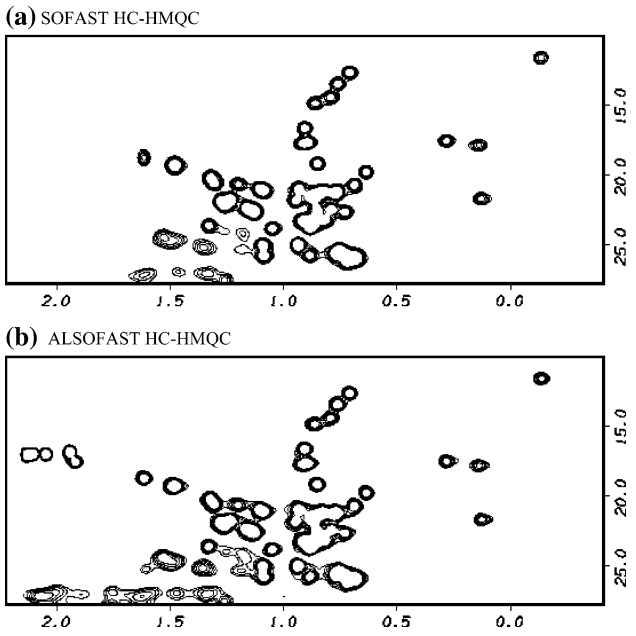


**Fig. 3** HC-HMQC spectra which were recorded in 0.25 mM [$^{13}$C,$^{15}$N]-FKBP-12 in 4 mm Shigemi micro sample tube on a Varian 600 MHz spectrometer which was equipped with a cold probe, sw = 11 kHz, sw1 = 32 ppm, # of $t_1$-increments = 64, data collection time of 1.3 min, (**a**) SOFAST HC-HMQC, excitation pulse: pc9 with 120°-excitation angle, 2 ppm width, centered at 0.6 ppm, echo pulse: rsnob with 2 ppm width centered at 0.6 ppm with (**b**) ALSOFAST HC-HMQC which was acquired with a selecting carbon editing of 20 ppm with the carbon carrier frequency set to 17.4 ppm, HC-HMQC excitation flip angle = 60°

positions at point f in Fig. 1. Hence, the combined effects of rf inhomogeneity and longitudinal relaxation during the intervals between time points f and j (Fig. 1) when magnetization of passive protons is inverted, appears to be the most plausible explanation for the apparent diminished performance of ALSOFAST at very short recycle delays (relaxation delay + $t_2$-acquisition time) as illustrated by the apparent drop in sensitivity gains reflected by the curves and squares in magenta in Fig. 4a and c. Moreover, several peaks in the SOFAST spectrum which is depicted in Fig. 2a appear to be more intense than the corresponding cross peaks in the ALSOFAST spectrum (Fig. 2b). In addition, the use of a non-selective echo pulse in the middle of $t_1$-evolution period (point f in Fig. 1) maintains the scalar $J_{HNH\alpha}$ coupling which contributes to a dephasing of the HN-multiple quantum coherence during $t_1$-evolution. A final concern pertains to possible sample heating by the high power proton rf pulses at short recycle delays. Using the rf performance specification on our Varian 600 MHz cold probe, the estimated power dissipation by the sum-total of all proton pulses in the ALSOFAST pulse sequence at a recycle delay of 0.2 s is about 2 mW which is still about 50-fold less than the power dissipation which is caused by the $^{15}$N-decoupling pulse train. The combination of coherence dephasing due to rf inhomogeneity and the unsuppressed $J_{HNH\alpha}$-coupling in $t_1$ contributes to a reduction in relative sensitivity in ALSOFAST HN-HMQC spectra especially in fully protonated samples at very short relaxation delays (see Fig. 4a). The integrated average intensities over all cross peaks multiplied by (2.0/recycle delay)$^{1/2}$ is depicted for Watergate (Sklenar et al. 1993) and water flip-back (Campbell-Burk et al. 1991; Kuboniwa et al. 1994) enhanced HN-HSQC (Bodenhausen and Ruben 1980) (green curve and triangles), the SOFAST NH-HMQC (blue curve and diamonds), and the ALSOFAST NH-HMQC (magenta curve and squares) (recycle delay represents the sum of the relaxation delay and the acquisition time $t_2$). At recycle delays in excess of 0.8 sec, the Watergate HN-HSQC experiment outperforms both SOFAST and ALSOFAST. But at recycle delays of less than 0.8 s both SOFAST and ALSOFAST begin to outperform the Watergate. Overall, SOFAST appears to outperform the ALSOFAST HMQ experiment at very short recycle delays protonated sample of FKBP-12.

For samples in which the proton density is reduced, such as in selectively protonated protein samples in a perdeuterated background, ALSOFAST HN-HMQC spectra tend to outperform both SOFAST HN-HMQC and the

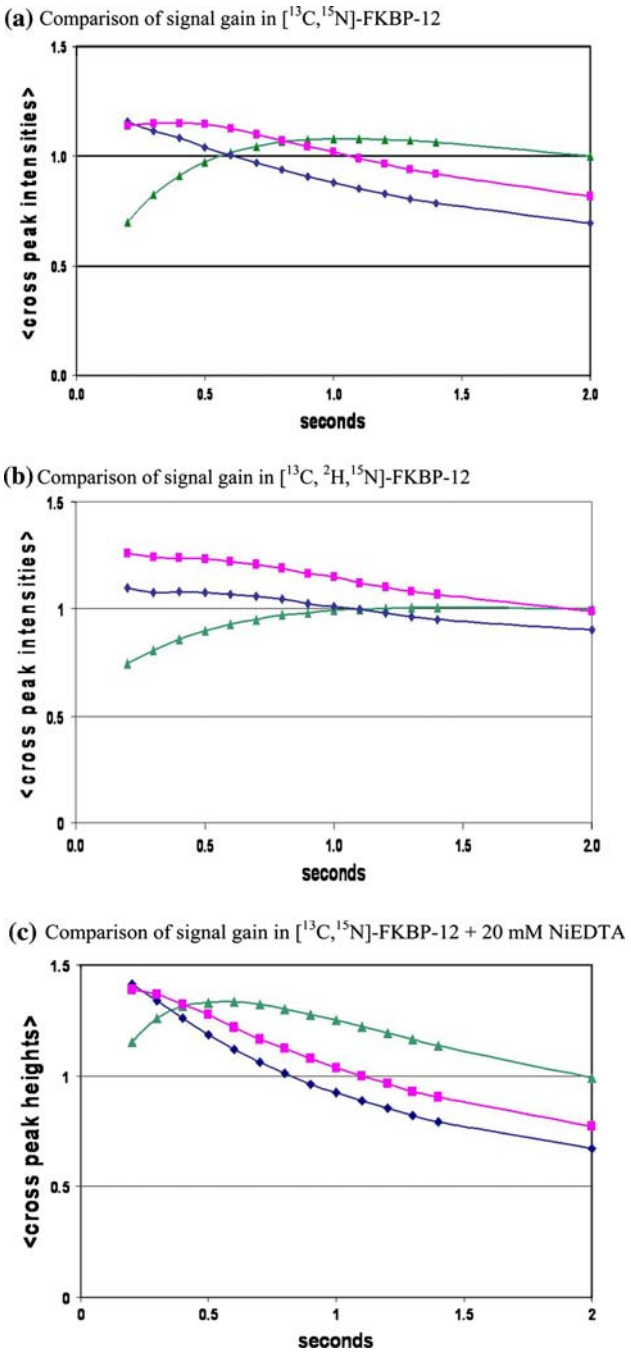


**Fig. 4** Illustration of signal gain by reducing the recycle delay (relaxation delay + acquisition time): average cross peak intensity multiplied by (2/recycle delay)$^{1/2}$ for ALSOFAST HN-HMQC (magenta squares), SOFAST HN-HMQC (blue diamonds), HN-HSQC Watergate (green triangles) in (**a**) 0.36 mM [$^{13}$C,$^{15}$N]-FKBP-12, (**b**) 0.25 mM [$^{13}$C,$^{2}$H,$^{15}$N]-[$^{1}$H]-ILV-FKBP-12 (protonation level of resonances between 2.0 and −0.5 ppm, ~38%), (**c**) 0.36 mM [$^{13}$C,$^{15}$N]-FKBP-12 + 20 mM NiEDTA acquisition time = 0.06 s. All spectra were recorded on a Varian Inova 600 spectrometer equipped with a cold probe. The spectra were recorded in an interleaved manner with the relaxation delay arrayed as follows: relaxation delay = 1.94, 0.14, 1.34, 0.24, 1.24, 0.34, 1.14, 0.44, 1.04, 0.54, 0.94, 0.64, 0.84, 0.74

HN-HSQC. This is illustrated in Fig. 4b, which depicts the sensitivity enhancement integrated over the entire HN-HMQC spectrum as a function of the recycling delay (relaxation delay + $t_2$-acquisition time). To demonstrate this, we show the sensitivity comparisons for a uniformly perdeuterated sample of FKBP-12 in which the methyl groups of isoleucine, leucine and valine residues were fully protonated, producing a residual protonation level of ~38% of protons which resonate upfield of 2.4 ppm. In this partially deuterated sample, the ALSOFAST HN-HMQC yields higher sensitivity than both SOFAST HN-HMQC and Watergate HN-HSQC at nearly all recycle delays (Fig. 4b). Similarly, a comparison of HN-HMQC and HN-HSQC spectra recorded in samples of protonated and partially deuterated Bcl-$_{XL}$ exhibited an overall sensitivity gain due to deuteration of around 35% (data not shown). This sensitivity enhancement is expected to be even greater when ALSOFAST is applied to higher molecular weight proteins, where the reduced INEPT interval between time points e and b (Fig. 1) limits signal loss due to transverse relaxation. Selective ILV side chain protonation enhances the performance of the ALSOFAST HN-HMQC experiment in two ways. First, because the methyl resonances provide a pool a magnetization which helps to repopulate magnetization of amide protons during the $t_2$-acquisition time and the relaxation delay. Second, the deuteration of the $H_\alpha$-protons eliminates the detrimental effects of the $J_{HNH\alpha}$-couplings. Even in ILV-protonated, perdeuterated protein samples, which are expressed in *E. coli*, all $H_\alpha$-sites are deuterated to a considerable extend (Crepsi et al. 1968; Metzler et al. 1996).

## Effect of a paramagnetic relaxation agent on performance of SOFAST and ALSOFAST

The addition of properly chelated $Ni^{++}$ ions to a protein solution produces a significant gain in sensitivity in HN-correlated spectra that are acquired with reduced recycle delays (Cai et al. 2006). As pointed out by Chen and coworkers, the short relaxation time of the unpaired electron in $Ni^{++}$ produces a reduction of the longitudinal proton relaxation time in macromolecules such as proteins without producing significant line broadenings. To test the effect of a $Ni^{++}$-containing relaxation enhancing agent on the performance of SOFAST and ALSOFAST, both SOFAST- and ALSOFAST HN-HMQC spectra were recorded in samples of uniformly [$^{13}$C,$^{15}$N]-FKBP-12, both in the absence and in the presence of 20 mM NiEDTA (Fig. 4c). At reduced recycle delays the presence of 20 mM NiEDTA produced significant signal enhancements in all three experiments. Interestingly, the performance of the HN-HSQC experiment is considerably enhanced

relative to both the SOFAST and ALSOFAST HN-HMQC at recycling delays of more than 0.5 s. As expected, the presence of a relaxation agent also alleviates saturation effects at short relaxation delays in the ALSOFAST HN-HMQC. The use of higher concentrations of NiEDTA is expected to further improve the performance of SOFAST and ALSOFAST, opening the possibility of recording data with the relaxation delay set to close to zero.

The presence of 20 mM NiEDTA in the NMR sample caused a 3% increase in the proton pulse width and a 2% drop in overall sensitivity. However, none of the observed HC nor NH-resonances (data not shown) experienced significant line broadening due to the presence of NiEDTA. Most likely, the bulk of the observed small drop in sensitivity is caused by the increase in ionic strength upon addition of 20 mM NiEDTA. Therefore, it is expected that the use of neutral NiDO2A will produce further gains in SOFAST and ALSOFAST spectra as described by Cai et al. (Cai et al. 2006). Alternatively, the increase in ionic strength caused by the addition of NiEDTA could possibly be compensated by the corresponding reduction of other salts in the NMR sample. The use of $Ni^{++}$ as a relaxation agent may be of particular benefit when ALSOFAST HN-HMQC spectra are recorded in the NMR screening mode, because this relaxation agent preferentially relaxes surface-exposed NHs which may come in spatial contact with an NMR screening hit (Shuker et al. 1996).

## Sensitivity enhanced ALSOFAST HN-HMQC

As demonstrated by (Schanda et al. 2005) SOFAST spectra can be recorded in the IPAP-mode (Ottiger et al. 1998). In the IPAP-mode of data collection no inverse decoupling is applied during the acquisition time which produces a two-fold drop in sensitivity. About 41% of this sensitivity can be recovered by the super-position of the two components of the NH-doublet by corresponding shifts of the two IPAP sub-spectra by $0.5 * J_{NH}$ (Schanda et al. 2005). Another 41% of signal can be gained by simultaneous sampling of the x- and y-component of the $t_1$-interferogram (sensitivity enhanced detection (Palmer et al. 1991; (Kay et al. 1992)). This can be accomplished by the protocol which is depicted below and which has been independently discovered by Brutscher and coworkers (Kern et al. 2008). Sensitivity enhanced detection in the IPAP HMQC experiment can be achieved by the application of an additional 90°-pulse on the X-channel at the start of $t_2$ (point l in Fig. 1a). At the onset of the 90°-pulse at point l in Fig. 1 the coherence of interest is represented by the product operators in Eq. 2:

$$H_x * \cos(\omega_1 * t_1) + 2 * H_y * N_x * \sin(\omega_1 * t_1) \quad (2)$$

The application of a nitrogen 90°-pulse along y at the start of $t_2$ converts the heteronuclear bilinear term in Eq. 2 to:

$$H_x * \cos(\omega_1 * t_1) + 2 * H_y * N_z * \sin(\omega_1 * t_1) \quad (3)$$

The second term in Eq. 3 now contributes additional signal to the dataset. This forms the basis of the depicted sensitivity enhanced detection scheme (Kern et al. 2008). The key task in making a productive use of the 2nd term in Eq. 3 is to devise a phase cycling scheme which permits the construction of a clean $t_1$-interferogram where the x-and y-components are properly disentangled. This is achieved by recording four fids per $t_1$-point where the phases of the nitrogen or carbon 90° pulses at the end of $t_1$ and the start of the detection period $t_2$ at point g and l in Fig. 1a, respectively, are altered as shown in Table 1.

The x-and y-components of the $t_1$-interferogram are constructed from the four acquired fids as follows:
x-component:

$$\begin{aligned} &\text{FID1} + \text{FID2} + \text{FID3}(+90^\circ\text{-phase shifted}) \\ &\quad - \text{FID4}(+90^\circ\text{-phase shifted}) \\ &\quad = 2 * H_x * \cos(\omega_1 * t_1) - 4 * H_x N_z * \cos(\omega_1 * t_1) \end{aligned}$$

y-component:

$$\begin{aligned} &\text{FID3} + \text{FID4} + \text{FID1}(+90^\circ\text{-phase shifted}) \\ &\quad - \text{FID2}(+90^\circ\text{-phase shifted}) \\ &\quad = -2 * H_x * \sin(\omega_1 * t_1) + 4 * H_x N_z * \sin(\omega_1 * t_1) \end{aligned}$$

The depicted sensitivity enhancement scheme has been independently developed and implemented in the SOFAST-HMQC experiment (Kern et al. 2008). In contrast to the implementation of the sensitivity enhancement scheme in the SOFAST-HMQC, which constructively adds TROSY anti-TROSY components to achieve another sensitivity gain approaching 1.41 in small proteins, the presented method simply aims at constructing a sensitivity HMQC-TROSY spectrum whereby the slower relaxing branch of the HN-doublet is retained and the anti-TROSY branch is discarded (Pervushin et al. 1997). Hence, the depicted ALSOFAST sensitivity enhancement scheme features an intrinsic loss in sensitivity relative the inverse decoupled ASOFAST HN-HQMC by a square root of two. In practice, the loss in sensitivity tends to be smaller due to the well-known TROSY effect (Pervushin et al. 1997) as illustrated in Table 2.

Sensitivity enhanced ALSOFAST HN-HMQC spectra were recorded in samples of [$^{13}$C,$^{15}$N]-FKBP-12 and [$^{13}$C,$^{2}$H,$^{15}$N]-[$^{1}$H]-ILV-FKBP-12 both at recycle delays of

**Table 1** Depiction of the rf phases $\Phi_6$ & $\Phi_7$ (see Fig. 1) and $^1$H-coherence at $t_2 = 0$ for the four FIDs which are acquired per $t_1$-point

| FID# | Φ6 | Φ7 | $^1$H-coherence at $t_2 = 0$ |
|---|---|---|---|
| 1 | x | y | $H_x * \cos(\omega_1 * t_1) + 2 * H_y * N_z * \sin(\omega_1 * t_1)$ |
| 2 | x | −y | $H_x * \cos(\omega_1 * t_1) - 2 * H_y * N_z * \sin(\omega_1 * t_1)$ |
| 3 | −y | −x | $-2 * H_y * N_z * \cos(\omega_1 * t_1) - H_x * \sin(\omega_1 * t_1)$ |
| 4 | −y | x | $+2 * H_y * N_z * \cos(\omega_1 * t_1) - H_x * \sin(\omega_1 * t_1)$ |

**Table 2** Sensitivity comparison of various excitation schemes. Ratios of average peak intensities (relative to average peak intensity of alsofast-ipap at $d_1 + at = 2.0$ s) (**a**) 0.378 mM [$^{13}C$,$^{15}N$]-FKBP12, (**b**) 0.258 mM [$^{13}C$,$^{2}H$,$^{15}N$,$^{1}H$-ILV]-FKBP12

| Experiment | 2 s | 0.3 s |
|---|---|---|
| *(a)* | | |
| Alsofast-se | 1.37 | 0.69 |
| Alsofast-ipap | 1.00 | 0.51 |
| Alsofast$^{15}$ N-dec | 1.80 | 0.92 |
| *(b)* | | |
| Alsofast-se | 1.41 | 0.62 |
| Alsofast-ipap | 1.00 | 0.47 |
| Alsofast$^{15}$ N-dec | 1.90 | 0.83 |

2.0 s and 0.3 s and compared with ALSOFAST HN-HMQC IPAP and the ALSOFAST HN-HMQC. The results are tabulated in Table 2. Sensitivity gains of 37% and 41% were achieved at a recycle delay of 2 s in the protonated and perdeuterated FKBP-12 samples, respectively, relative to IPAP. At a recycle delay of 0.3 s, the Sensitivity enhanced detection scheme yielded gains of 35% and 32% in the protonated and perdeuterated samples, respectively. This result illustrates the efficiency of the new sensitivity enhancement protocol which, in contrast to the coherence transfer based sensitivity enhancement scheme (Kay et al. 1992), features only one reverse INEPT interval between the end of the evolution period $t_1$ and the beginning of the detection period $t_2$. As expected, without the addition of the anti-TROSY component as depicted by Brutscher and coworkers (Schanda et al. 2005; Kern et al. 2008), the sensitivity enhanced ALSOFAST HN-HMQC spectra are less sensitive than their $^{15}$N-decoupled counterparts. However, due to the TROSY relaxation effect the sensitivity difference is smaller than the intrinsic factor of 1.41.

## Amino acid type editing in ALSOFAST HC-HMQC

In the constant time version of the ALSOFAST HC-HMQC experiment which is depicted in Fig. 1b, the constant time evolution interval $T_c$ is reduced by a factor of 2 to $1/(2 * J_{CC})$ relative to the constant time SOFAST HC-HMQC (Schanda et al. 2005). This modification provides an elegant means for amino acid type editing in methyl group containing residues, because it ensures that the signals of all methyl carbons which experience the effect of a one-bond $^{1}J_{CC}$-coupling are suppressed. Hence, in the absence of homonuclear decoupling, all methyl resonances with the exception of the methionine $\varepsilon$-methyls are suppressed, allowing a convenient detection of methionine methyls in uniformly $^{13}$C-labeled protein samples (see cyan contours in Fig. 5a). The employment of CA-WURST homonuclear decoupling (Kupce and Freeman 1996) during the constant time evolution period (interval e–g in Fig. 1b) allows decoupling of carbons that resonate in a targeted frequency range. For example, applying a CA-WURST pulse train during the constant time $t_1$-evolution with a band width of 10 ppm and a resonance frequency of 71 ppm yields an ALSOFAST HC-HMQC spectrum which only contains resonances from threonines (Fig. 5a: red contours) and methionines (Fig. 5a: cyan contours). Applying a CA-WURST pulse of 12 ppm band width and a resonance frequency of 53 ppm produces a spectrum that only contains resonances from alanines (Fig. 5a: green contours) and the ubiquitous methionine residues. This implementation of amino acid type editing of methyl resonances is analogous to the approach by Brutscher and coworkers (Van Melckebeke et al. 2004). To minimize effects of Bloch–Siegert shift distortions by the CA-WURST decoupling, a compensated CA-WURST decoupling pulse is applied in parallel at the mirror image resonance offset and with inverted sign of the frequency sweep (Van Melckebeke et al. 2004). It is even possible to apply higher selectivity homonuclear decoupling pulse trains featuring a band width of only 4 ppm. This yields HC-correlation spectra which feature only methyl resonances of carbons which are chemically bonded to a carbon which resonates at a target resonance of $X \pm 2$ ppm. This permits a rapid identification of the approximate chemical shifts of carbons which are adjacent to a targeted methyl. Knowing the approximate chemical shift of these carbons may be of particular value in NOE-matching based structure determination of protein:ligand complexes (Constantine et al. 2006), since it will enable a user to impose additional boundary conditions to the NOE-matching filters. Figure 5b depicts the constant time ALSOFAST HC-HMQC spectrum with a 4 ppm CA-WURST decoupling centered at 39 ppm and in Fig. 5c the selective carbon decoupling pulse trains during the constant time $t_1$-evolution period was shifted upfield by 3 ppm. This small shift in the homo-nuclear carbon decoupling field gave rise to a dramatic change in the pattern of observed methyl HC-resonances.

## Conclusions

ALSOFAST-HMQC provides a new tool for biomolecular NMR applications which exhibits a considerable degree of complementarities to the novel SOFAST-HMQC experiment (Schanda and Brutscher 2005; Schanda et al. 2005; Kern et al. 2008). In contrast to the SOFAST HN-HMQC, the ALSOFAST HN-HMQC experiment offers uniform HN-proton excitation of resonances of interest regardless of their chemical shifts, which may be of particular value in proteins or nucleic acids that feature large secondary HN-chemical shifts. However, uniform excitation of

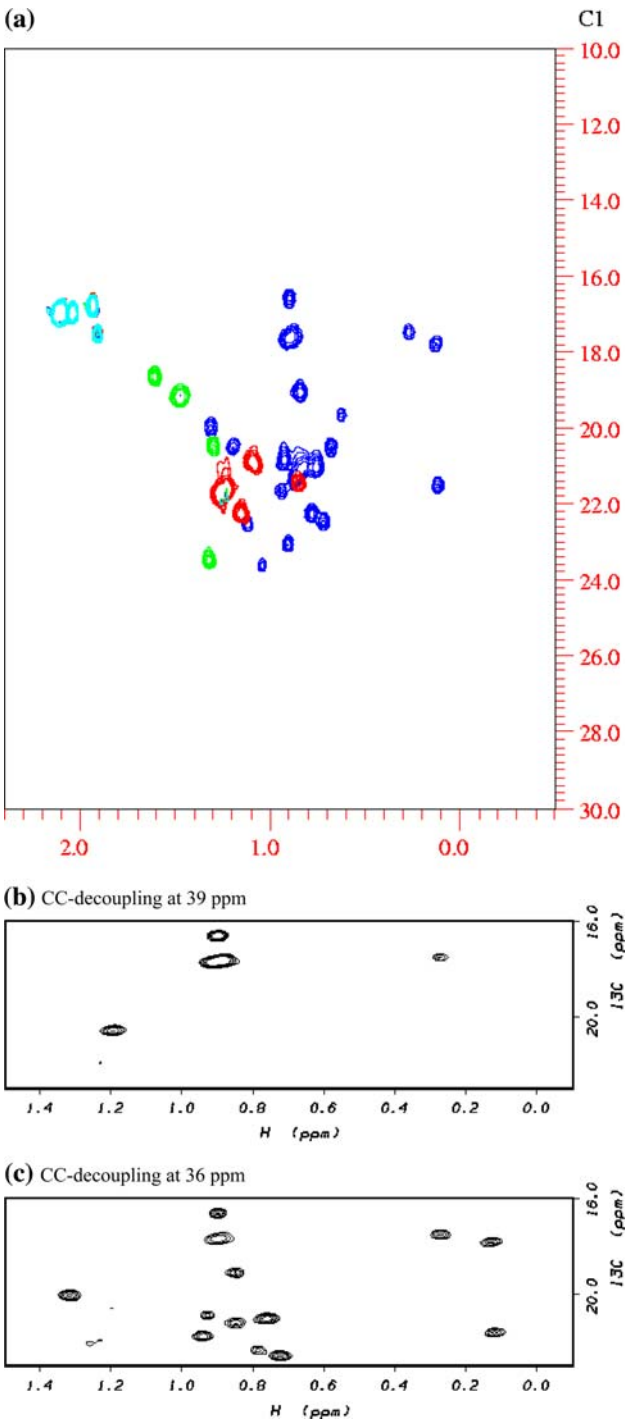


◀**Fig. 5** (**a**) Superposition of carbon-edited constant time ALSOFAST HC-HMQC spectra which were obtained in a sample of 0.36 mM uniformly [$^{13}$C,$^{15}$N]-FKBP-12, all spectra were collected in 1 min each. The color-coding of cross peaks is a follows: methionine = cyan, alanine = green, threoneine = red, valines = blue (contains some contamination of leucine delta methyls). The $^{13}$C homodecoupling was done with a CA-WURST pulse train whose band width was set to 10 ppm for thr $C_\beta$-decoupling and 12 ppm for ala $C_\alpha$ and val $C_\beta$-decoupling with an inversion pulse width of 5.0 ms. The decoupling pulse frequencies were set to 71.0 and −40.0 ppm for thr $C_\beta$-decoupling, 53.0 and −22.0 ppm for ala $C_\alpha$-decoupling and 36.0 and −5.0 ppm for val $C_\beta$-decoupling. The carbon frequency was set to 15.5 ppm. The duration of the soft water inversion pulse was set to 1,680 μs, and the g3-inversion pulse was set to an excitation band width of 20 ppm. Expanded region of constant time ALSOFAST HC-methyl correlation spectrum with a selective $^{13}$C homodecoupling width a decoupling band width of 4 ppm and the decoupling pulse train centered at (**b**) 39 ppm and (**c**) 36 ppm

HN-resonances in ALSOFAST requires the application of a larger number of proton pulses which has the effect of attenuating signal gains in the central region of the amide proton spectrum at relaxation delays which are considerably shorter than the proton $T_1$-relaxation times. This shortcoming of the ALSOFAST technique is reduced in deuterated proteins. A particular high degree of complementarity is realized between the SOFAST- and ALSOFAST HC-HMQC experiment. While the SOFAST HC-HMQC achieves selectivity of excitation by selective proton pulses, in the ALSOFAST HC-HMQC selectivity of excitation is achieved by a selective carbon population inversion pulse in the center of the INEPT interval (point c in Fig. 1b). As a result, SOFAST HC-HMQC permits high throughput acquisition of HC-spectra of protons which resonate in a targeted spectral range while the corresponding frequency editing by carbon pulses may render ALSOFAST HC-HMQC spectroscopy more suitable for rapid acquisition of carbon-type edited spectra. In particular, the constant time version of the ALSOFAST HC- HMQC offers an elegant means for editing methyl resonances based on the resonance frequencies of their chemically bonded carbon, which in some cases allows amino acid type editing of methyl resonances. The ALSOFAST HN-HMQC experiment may have some advantages for data collection in perdeuterated proteins samples of higher molecular weight proteins, where the partial deuteration of aliphatic protons may mitigate the relative loss of signals at shorter relaxation delay, and the relatively shorter HN-INEPT interval in ALSOFAST may reduce signal loss due to $T_2$-relaxation. Finally, both the SOFAST and ALSOFAST-HMQC pulse sequence permit the implementation of a novel sensitivity enhancement scheme in a straightforward manner without the need for inserting additional delays between the end of $t_1$ and the onset of $t_2$. This affords the realization of sensitivity gains close to the theoretical limit of 41%. Finally, the use of paramagnetic relaxation agents which accelerate the longitudinal $T_1$ relaxation of protons is expected to further enhance the sensitivity of both SOFAST and ALSOFAST-HMQC spectra in a comparable manner. The use of paramagnetic relaxation agents may prove of particular value in detecting protein binding of ligands by chemical shift perturbation mapping (Gorlach et al. 1992; Shuker et al. 1996) because highly polar agents such as NiEDTA or NiDO2A preferentially enhance NH-protons on the protein surface (Cai et al. 2006).

**Acknowledgments** All isotopically enriched protein samples have been expressed and purified by Valentina Goldfarb. The author acknowledges William J. Metzler's assistance in editing the manuscript.

## References

Atreya HS, Szyperski T (2005) Rapid NMR data collection. Meth Enzymol 394:78–108

Bodenhausen G, Ruben DJ (1980) Natural abundance nitrogen-15 NMR by enhanced heteronuclear spectroscopy. Chem Phys Lett 69:185–189

Cai S, Seu C, Kovacs Z, Sherry AD, Chen Y (2006) Sensitivity enhancement of multidimensional NMR experiments by paramagnetic relaxation effects. J Am Chem Soc 128:13474–13478

Campbell-Burk S, Domaille P, Mueller L (1991) Observation of labile amide protons via indirect detection of nitrogen-15 single-quantum transitions. J Magn Reson 93:171–177 1969–1992

Constantine KL, Davis ME, Metzler WJ, Mueller L, Claus BL (2006) Protein-ligand NOE matching: a high-throughput method for binding pose evaluation that does not require protein NMR resonance assignments. J Am Chem Soc 128:7252–7263

Crepsi HL, Rosenberg RM, Katz JJ (1968) Proton magnetic resonance of proteins fully deuterated except for 1H-leucine side chains. Science 161:795–796

Emsley L, Burghardt I, Bodenhausen G (1990) Double selective inversion in NMR and multiple quantum effects in coupled spin systems. J Magn Reson 90:214–220

Ernst RR, Anderson WA (1966) Application of Fourier transform spectroscopy to magnetic resonance. Rev Sci Instrum 37:93–102

Freeman R, Kupce E (2003) New methods for fast multidimensional NMR. J Biomol NMR 27:101–114

Freeman R, Mareci TH, Morris GA (1981) Weak satellite signals in high-resolution NMR spectra: separating the wheat from the chaff. J Magn Reson 42:341–345

Gorlach M, Wittekind M, Beckman RA, Mueller L, Dreyfuss G (1992) Interaction of the RNA-binding domain of the hnRNP C proteins with RNA. EMBO J 11:3289–3295

Hwang T-L, Shaka AJ (1995) Water suppression that works. Excitation sculpting using arbitrary waveforms and pulsed field gradients. J Magn Reson A 112:275–279

Kay LE, Keifer P, Saarinen T (1992) Pure absorption gradient enhanced heteronuclear single quantum correlation spectroscopy with improved sensitivity. J Am Chem Soc 114:10663–10665

Kern T, Schanda P, Brutscher B (2008) Sensitivity enhanced IPAP-SOFAST-HMQC for fast-pulsing 2D NMR with reduced radiofrequency load. J Magn Reson 190:333–338

Kuboniwa H, Grzesiek S, Delaglio F, Bax A (1994) Measurement of $H^N$–$H^z$ J couplings in calcium-free calmodulin using new 2D and 3D water-flip-back methods. J Biomol NMR 4:871–878

Kupce E, Freeman R (1996) Optimized adiabatic pulses for wide-band spin inversion. J Magn Reson A 118:299–303

Kupce E, Freeman R (2007) Fast multidimensional NMR by polarization sharing. Magn Reson Chem 45:2–4

Metzler WJ, Wittekind M, Goldfarb V, Mueller L, Farmer BTII (1996) Incorporation of 1H/13C/15 N-{Ile, Leu, Val} into a perdeuterated, 15 N-labeled protein: potential in structure determination of large proteins by NMR. J Am Chem Soc 118:6800–6801

Mueller L (1979) Sensitivity enhanced detection of weak nuclei using heteronuclear multiple quantum coherence. J Am Chem Soc 101:4481–4484

Ottiger M, Delaglio F, Bax A (1998) Measurement of J and dipolar couplings from simplified two-dimensional NMR spectra. J Magn Reson 131:373–378

Palmer AGIII, Cavanagh J, Wright PE, Rance M (1991) Sensitivity improvement in proton-detected two-dimensional heteronuclear correlation NMR spectroscopy. J Magn Reson 93:151–170

Pervushin K, Riek R, Wider G, Wuthrich K (1997) Attenuated T-2 relaxation by mutual cancellation of dipole-dipole coupling and chemical shift anisotropy indicates an avenue to NMR structures of very large biological macromolecules in solution. Proc Natl Acad Sci USA 94:12366–12371

Pervushin K, Voegeli B, Eletsky A (2002) Longitudinal 1H relaxation optimization in TROSY NMR spectroscopy. J Am Chem Soc 124:12898–12902

Ross A, Salzmann M, Senn H (1997) Fast-HMQC using Ernst angle pulses: an efficient tool for screening of ligand binding to target proteins. J Biomol NMR 10:389–396

Schanda P, Brutscher B (2005) Very fast two-dimensional NMR spectroscopy for real-time investigation of dynamic events in proteins on the time scale of seconds. J Am Chem Soc 127:8014–8015

Schanda P, Kupce E, Brutscher B (2005) SOFAST-HMQC experiments for recording two-dimensional deteronuclear correlation spectra of proteins within a few seconds. J Biomol NMR 33:199–211

Shuker SB, Hajduk PJ, Meadows RP, Fesik SW (1996) Discovering high-affinity ligands for proteins: SAR by NMR. Science 274:1531–1534

Sklenar V, Piotto M, Leppik R (1993) Gradient-tailored water suppression for proton-nitrogen-15 HSQC experiments optimized to retain full sensitivity. J Magn Reson A 102:241–245

Van Melckebeke H, Simorre J-P, Brutscher B (2004) Amino acid-type edited NMR experiments for methyl–methyl distance measurement in 13C-labeled proteins. J Am Chem Soc 126:9584–9591